Supporting Information

Geng et al. 10.1073/pnas.1319441111

SI Text

1. Discussion

1.1. $\delta^{15}N$ of NO_x and Atmospheric Nitrate. NO_x is mainly produced from combustion and biogenic processes. Before the Industrial Revolution, soil biogenic emissions, biomass burning, and lightning were the dominant NO_x sources. These are referred to as natural sources. After the Industrial Revolution, human activities started to dominate NO_x emissions mainly through fossil fuel combustion (1). Human activities have also altered the properties of agricultural soil by adding synthesized nitrogen fertilizer. In this research, NO_x emitted from *N*-fertilized soil is considered to be anthropogenic in origin.

The values of $\delta^{15}N(NO_x)$ from different sources are listed in Table S1. NO_x emitted from *N*-fertilized and unfertilized soil possesses negative $\delta^{15}N$, which is expected because NO_x produced in soil is through biogenic denitrification processes that preferentially consume ^{14}N (2). Biomass burning produces NO_x primarily through the oxidation of nitrogen contained in biomass (fuel NO_x), as the temperature of biomass burning is not high enough to convert atmospheric N_2 and O_2 to NO_x (thermal NO_x) (3). Therefore, $\delta^{15}N(NO_x)$ from biomass burning is determined by the ^{15}N abundance of the biomass, and was predicted to be negative (4) as *N*-nutrition from nitrification possesses negative $\delta^{15}N$ values (−10 ‰ to −7 ‰) (5).

NO_x produced from fossil fuel combustion contains both fuel NO_x and thermal NO_x (6). The values of $\delta^{15}N$ are thus determined by the abundance of ^{15}N in fossil fuel, and the combustion temperature. Therefore, $\delta^{15}N(NO_x)$ from fossil fuel combustion is difficult to predict, as ^{15}N in fuel may vary geographically and the combustion temperature also varies. Existing measurements reported $\delta^{15}N(NO_x)$ varying from −19 ‰ to 26 ‰, but most often reported positive $\delta^{15}N(NO_x)$ values (Table S1 and references therein).

Although large uncertainties exist, in part due to the incomplete collection of NO_x during sampling processes, available data (Table S1) generally suggest $\delta^{15}N(NO_x)$ from fossil fuel combustion is higher than that from natural sources. In addition, measurements of $\delta^{15}N$ from atmospheric NO_x and nitrate, which reflects a combination of fossil fuel and natural sources, indicate higher $\delta^{15}N$ in areas with more fossil fuel combustion compared with relatively pristine regions (e.g., refs. 6–9). Therefore, fossil fuel combustion most likely produces NO_x with higher $\delta^{15}N$ than natural sources.

1.2. NO_x from Fossil Fuel Combustion and *N*-Fertilized Soil. To further examine whether or not NO_x source change (additional fossil fuel combustion emissions and *N*-fertilized soil emissions) could cause the decrease in ice core $\delta^{15}N(NO_3^-)$, based on our ice core data reported in this work, we calculated the $\delta^{15}N$ value of NO_x derived from fossil fuel combustion following Hastings et al. (10), and calculated the contribution of *N*-fertilized soil NO_x to Greenland ice core nitrate following Felix et al. (11).

Greenland nitrate concentrations in the present day are about double those in the preindustrial period. The additional nitrate is mainly from two anthropogenic sources, fossil fuel combustion and *N*-fertilized soil. Assuming that there is no nitrogen fractionation from the source (NO_x) to sink (nitrate in ice core), given the measured value of $\delta^{15}N(NO_x)$ from *N*-fertilized soil (−48.9 ‰ to −19.9 ‰, Table S1), the value of $\delta^{15}N(NO_x)$ from fossil fuel combustion can be calculated assuming mass balance:

$$C_{PD} \times \delta^{15}N_{PD} = C_{PI} \times \delta^{15}N_{PI} + C_{FF} \times \delta^{15}N_{FF} + C_{NS} \times \delta^{15}N_{NS} \quad \textbf{[S1]}$$

$$C_{PD} - C_{PI} = C_{FF} + C_{NS}, \quad \textbf{[S2]}$$

where C_{PD} and $\delta^{15}N_{PD}$ are the average concentration (129.6 μg L^{-1}) and $\delta^{15}N$ (−1.0 ‰) of nitrate in the present day (using the post-1970 averages); C_{PI} and $\delta^{15}N_{PI}$ are the average concentration (58.2 μg L^{-1}) and $\delta^{15}N$ (13.4 ‰) of nitrate in preindustrial period (using the pre-1850 averages); C_{FF} and $\delta^{15}N_{FF}$ are the concentration and $\delta^{15}N$ of nitrate originating from fossil fuel combustion; C_{NS} and $\delta^{15}N_{NS}$ are the concentration and $\delta^{15}N$ of nitrate originating from *N*-fertilized soil. The ratio of C_{FF} to C_{NS} (i.e., the relative contributions of fossil fuel combustion and *N*-fertilized soil emission to Greenland ice core nitrate) can be estimated from the present day contributions of fossil fuel combustion and *N*-fertilized soil to global NO_x inventory (25.6 TgN y^{-1} vs. 2.5~4.5 TgN y^{-1}) (1).

Combining Eqs. **S1** and **S2** to solve for $\delta^{15}N_{FF}$ yields $\delta^{15}N_{FF}$ of −12.8 ‰ or −9.8 ‰ respective to a $\delta^{15}N_{NS}$ value of −19.9 ‰ or −48.9 ‰. This result is much lower than most of the measured $\delta^{15}N(NO_x)$ from fossil fuel combustion (Table S1), and is ~23 ‰ lower than the pre-1850 $\delta^{15}N(NO_3^-)$ average of 13.4 ‰ [also 23 ‰ lower than $\delta^{15}N$ of NO_x from natural sources, assuming that pre-1850 ice core $\delta^{15}N()$ represents $\delta^{15}N$ signal of natural NO_x source (10–12)]. Therefore, this calculation confirms that NO_x emissions from fossil fuel combustion is not responsible for the observed decrease in $\delta^{15}N(NO_3^-)$.

N-fertilized soil produces NO_x with very low $\delta^{15}N$ values (Table S1), so if *N*-fertilized soil had contributed significant NO_x to the Greenland nitrate [two to four times higher than that predicted from NO_x inventories, suggested by Felix et al. (11)], it would probably account for the observed decrease in $\delta^{15}N(NO_3^-)$. Following the idea of the "two end-member mixing model" (11), but involving ice core nitrate concentration record for a better constraint, we assumed $\delta^{15}N_{FF} = \delta^{15}N_{PI}$ in Eqs. **S1** and **S2** and then solved the two unknowns C_{FF} and C_{NS} by varying $\delta^{15}N_{NS}$ from −20 ‰, −27 ‰ to −49 ‰ following Felix et al. (11). As a result, we found NO_x from *N*-fertilized soil should have contributed 43.2%, 35.7%, and 23.2% (C_{NS}/C_{PD}), respective to different $\delta^{15}N_{NS}$ values, to Greenland ice core nitrate after 1970 Christian Era (C.E.) to explain the observed decrease in $\delta^{15}N(NO_3^-)$ from 1850 to 1970. This result is similar to the result from Felix et al. (11). Relatively, the respective (to different $\delta^{15}N_{NS}$ values) contribution of NO_x from fossil fuel combustion to Greenland ice core nitrate after 1970 was calculated (C_{FF}/C_{PD}) to be 11.9%, 19.4%, and 31.9%. So, NO_x from fossil fuel combustion and that from *N*-fertilized soil together contribute ~55.1% of Greenland ice core nitrate after 1970, consistent with the ice core nitrate concentration record that shows a slightly over two times increase in nitrate concentration from 1890 to 1970 (Figs. 1 and 2*C*). The ratio of the contributions from *N*-fertilized soil and fossil fuel combustion NO_x sources to Greenland ice core nitrate after 1970 was then calculated to be 3.2, 1.8, and 0.72 respective to different $\delta^{15}N_{NS}$ values. In other words, *N*-fertilized soil must have produced NO_x equivalent to 72–320% of that produced by fossil fuel combustion after 1970 to explain the observed ~14.4 ‰ decrease in $\delta^{15}N(NO_3^-)$ from 1850 to 1970 C.E. This is 4–32 times higher than previous model estimates (1).

It has to be emphasized that all of the above calculations (with somewhat unrealistic results) assume that there is no nitrogen isotope fractionation from NO_x source to sink (nitrate in ice core), which is clearly not the case as demonstrated in this study.

In addition, the other assumption/adoption in Felix et al. (11) that the measured pre-1850 mean value of $\delta^{15}N(NO_3^-)$ represents the $\delta^{15}N$ value of NO_x from biomass burning and equals that from fossil fuel combustion is problematic due at least in part to the enrichment of $\delta^{15}N$ of snow nitrate from postdepositional loss.

1.3. Calculating Annual $[H^+]$ and $[HNO_3]$. From the profiles of the chemical impurities obtained from Core 1, we calculated the annual concentration of H^+ in precipitation from 1772 to 2006 through ion balance:

$$[H^+] = [Cl^-] + [NO_3^-] + [SO_4^{2-}] - [Na^+] - [NH_4^+] - [K^+] - [Mg^{2+}] - [Ca^{2+}]. \quad \textbf{[S3]}$$

All concentrations are in microequivalents per liter. This method was demonstrated to yield $[H^+]$ record in good agreement with actual measurement of ice core $[H^+]$ by a continued flow system attached with a glass pH electrode (13). Organic acids are also present in ice cores, but ignoring their contributions only induces negative H^+ values in years with large biomass burning impacts and will not affect the overall trends of H^+ (13, 14).

In addition, we calculated the concentration of acid form nitrate (HNO_3) in the ice core from 1772 to 2006 by mass balance:

$$[HNO_3] = [H^+] - (\text{nss}[SO_4^{2-}] - [NH_4^+]), \quad \textbf{[S4]}$$

where $\text{nss}[SO_4^{2-}]$ is the difference between total sulfate concentration and sea salt sulfate that is $0.25 \times [Na^+]$ (15). We first calculated $\text{nss}[SO_4^{2-}]$ in nanograms per liter using the SO_4^{2-}/Na^+ weight ratio of 0.25, and then converted that to microequivalents per liter. This calculation assumes ice core acidity is dominated by sulfuric acid and nitric acid. The calculated concentration of HNO_3 represents the contribution of gas-phase nitrate to total ice core nitrate concentrations.

1.4. Fractionation in Partitioning of $HNO_{3(g)}$ and $p\text{-}NO_3^-$. In the atmosphere, nitrate partitions between the gas and aerosol phases (in aerosols, nitrate exists mainly in the aqueous phase of the surface liquid layer of aerosols) and the partial vapor pressure of $HNO_{3(g)}$ are determined by the aerosol liquid water content and effective Henry's law constant (16).

$$[\text{Nitrate}]_T = \frac{P_{HNO_3}}{RT} + [\text{Nitrate}]_{aq} \times W_L, \quad \textbf{[S5]}$$

where $[\text{Nitrate}]_T$ represents the total nitrate concentration in the atmosphere (moles per liter of air); P_{HNO3} represents the partial pressure of $HNO_{3(g)}$, $[\text{Nitrate}]_{aq}$ represents the concentration of nitrate in aqueous phase ($p\text{-}NO_3^-$, in moles per liter of water); and W_L is the liquid water content of aerosols (grams per liter of air). The relationship between $[\text{Nitrate}]_{aq}$ and P_{HNO3} follows Henry's law:

$$[\text{Nitrate}]_{aq} = H \times \left(1 + \frac{K_{nl}}{[H^+]}\right) \times p_{HNO_3} \approx \frac{3.2 \times 10^6}{[H^+]} \times p_{HNO_3}. \quad \textbf{[S6]}$$

H is the Henry's law constant for nitric acid (2.1×10^5 M atm^{-1} at 298 K); K_{n1} is the dissociation constant for nitric acid (15.4 M at 298 K). For simplicity, ideal conditions were assumed so that Henry's law can be applied without involving activity coefficients. The implications of this assumption for our results are explored below.

As precipitation dilutes $[H^+]$ compared with aerosols, we scaled the calculated H^+ concentration to aerosol acidity according to an approximate median aerosol pH of 4 [aerosol pH varies from 3 to 5 for aerosol diameters (D_p) larger than 2 μm, and pH = 2–5 with $D_p < 2$ μm (17)]. Typical liquid water content (W_L) of aerosol was estimated to be in the order of 10^{-6} g m^{-3} of air (17, 18). Combining Eqs. **S5** and **S6**, we calculated f (Eq. **4**) in each year from 1772 to 2006. To avoid the impacts of extremely elevated H^+ concentrations caused by volcanic eruptions and negative H^+ concentrations caused by ignoring organic acid from large biomass burning events on the calculations of f, we smoothed out such events by replacing their H^+ values with the average of H^+ concentrations in years before and after each individual event. Then we apply f to the fractionation model equations, to calculate $\delta^{15}N(HNO_{3(g)})$ and $\delta^{15}N(p\text{-}NO_3^-)$ in each year.

The value of the equilibrium fractionation constant between atmospheric $HNO_{3(g)}$ to $p\text{-}NO_3^-$ is unknown. A field study in Antarctica, where $HNO_{3(g)}$ evaporates from snow grain surfaces, calculated an ε value of −8.5 ‰ at −10 °C (19). A laboratory study on the partitioning of nitrate between $HNO_{3(g)}$ and NH_4NO_3 particles calculated an ε value of −21 ‰ at 25 °C (20). We applied the ε values from these two analog cases to our model for best estimates. In the purpose of simplification, we fixed the model temperature at 298 K. The calculated fractionation result, denoted as $\delta^{15}N(NO_3^-)_m$, is represented by the difference between $\delta^{15}N(HNO_{3(g)})$ and $\delta^{15}N(p\text{-}NO_3^-)$. The modeled $\delta^{15}N(NO_3^-)$ plotted in Fig. 2*D* was adjusted by adding the observed pre-1850 mean of $\delta^{15}N(NO_3^-)$ to the calculated $\delta^{15}N(NO_3^-)_m$ anomaly from 1772 to 2006, where the anomaly is relative to the pre-1850 mean of $\delta^{15}N(NO_3^-)_m$. The ε value of −21 ‰ with a fixed model temperature at 298 K gave the best result compared with the observations as shown in Fig. 2*D*. Using $\varepsilon = -8.5$ ‰ underestimates the magnitude of the $\delta^{15}N(NO_3^-)$ decrease by 5.9 ‰, which is probably because the snow surface is more like a disorganized layer instead of a liquid layer as on the surface of aerosols and thus the fractionation process occurring at the snow surface may be quite different from that in the aerosol surface.

To test the sensitivity of the modeled $\delta^{15}N(NO_3^-)$ to temperature, we performed preliminary sensitivity studies by varying our model temperature with $\varepsilon = -21$ ‰. We found that at lower temperatures (<298 K), the magnitude of the decrease of modeled $\delta^{15}N(NO_3^-)$ from 1850 to 1970 is reduced due to the temperature dependence of the Henry's law coefficient and the dissociation constant of nitric acid. However, when varying the model temperature, two other model parameters must be also varied: aerosol liquid water content (W_L) (18) and the equilibrium isotope fractionation constant. Unfortunately, quantitative information regarding the temperature dependence of aerosol water liquid content and the equilibrium fractionation factor between atmospheric $HNO_{3(g)}$ to $p\text{-}NO_3^-$ are unknown.

In addition, when calculating f using Eqs. **S5** and **S6**, we assumed ideal conditions so that Henry's law can be applied. In reality, activity coefficients of ions in aerosol must be considered because atmospheric aerosols are usually concentrated solutions that deviate from ideality. To examine the implications of this assumption on our conclusions, we used an aerosol thermodynamic equilibrium model, ISORRPIA II (21), to calculate f in the preindustrial period and in the 1970s, and then applied the calculated f to the Rayleigh fractionation model to calculate the decrease in $\delta^{15}N(NO_3^-)$ from the preindustrial period to the 1970s. Assuming that the partitioning of $HNO_{3(g)}$ and $p\text{-}NO_3^-$ and the fractionation between them mainly occur in their source regions, we used the average concentrations of Cl^-, NO_3^-, SO_4^{2-}, Na^+, K^+, Mg^{2+}, and Ca^{2+} from the model's default input data for continental urban and rural scenarios to represent present-day values, and scaled them down to estimate their values in the 1970s and in the preindustrial period based on their concentration changes documented by the ice core record shown here. Due to the very low abundance of NH_4^+ in Greenland ice cores

and the fact that the ice core record does not capture the increasing trend in NH_4^+ expected from anthropogenic emission changes (22), we adjusted the concentration of NH_4^+ in different periods based on the NH_3 emission inventory data in the United States (23). At 298 K, and with 90% relative humidity, the decrease in $\delta^{15}N(NO_3^-)$ was calculated to be 36.2 ‰ with $\varepsilon = -21$ ‰ and 14.2 ‰ with $\varepsilon = -8.5$ ‰. The magnitude of the calculated decrease in $\delta^{15}N(NO_3^-)$ increases with decreasing temperature and/or relative humidity. The decrease in $\delta^{15}N(NO_3^-)$ calculated by applying the ISORROPIA II model is much larger than that (15.6 ‰ with $\varepsilon = -21$ ‰ and 8.9 ‰ with $\varepsilon = -8.5$ ‰) calculated by applying Eqs. **S5** and **S6**, suggesting that our assumption (ideal conditions) may lead to an underestimate of the decrease originating from the acidity change. We note that our model does not consider the effect of increases in fossil fuel NO_x, which is expected to increase $\delta^{15}N(NO_3^-)$.

1.5. Fractionation in NO_x Cycling. Atmospheric NO and NO_2 cycle rapidly in the presence of O_3 (HO_2/RO_2) and sunlight:

$$NO + O_3 \rightarrow NO_2 + O_2 \qquad \textbf{[SR1]}$$

$$NO + HO_2 \rightarrow NO_2 + OH \qquad \textbf{[SR2]}$$

$$NO + RO_2 \rightarrow NO_2 + RO \qquad \textbf{[SR3]}$$

$$NO_2 \xrightarrow{h\nu} NO + O \qquad \textbf{[SR4]}$$

NO_2 is removed from this cycle by being converted to HNO_3. The conversion of NO_2 to HNO_3 is considered to have little or no nitrogen isotope fractionation (24, 25); thus $\delta^{15}N$ of total nitrate should reflect that of NO_2. Based on a box model (24), the abundance of ^{15}N in NO_2 can be expressed as the following equation:

$$\left[{}^{15}NO_2\right] = \left[{}^{15}NO_x\right] - \frac{\left[{}^{15}NO_x\right]}{1 + \alpha \cdot \frac{[NO_2]}{[NO]}}, \qquad \textbf{[S7]}$$

where α is the equilibrium fractionation factor between NO and NO_2. Assuming steady state between NO_2 and NO in NO_x cycling, the ratio of NO_2 to NO can be calculated as:

$$[NO_2]/[NO] = \frac{k_1 \times [O_3]}{k_2}, \qquad \textbf{[S8]}$$

where k_1 and k_2 represent the rate constants of Reactions **SR1** and **SR4**, respectively. To simplify the calculation, we ignored the conversion of NO to NO_2 through Reactions **SR2** and **SR3** as Reaction **SR1** dominates the conversion (80–90%) throughout most of the troposphere (26).

Using model calculated O_3 concentrations for the present day (42 ppbv) and the preindustrial period (24 ppbv) in northern midlatitudes (30°N~60°N) (27), and $\alpha = 1.018$ (25), we calculated a decrease in $\delta^{15}N(NO_2)$ of 2.2 ‰ from preindustrial period to the present day owing to this O_3 concentration increase. Including the concentration change of NO_x from preindustrial period to the present day based on GEOS-Chem model input data (27) did not change this result. The increase in tropospheric O_3 abundance explains up to ~15% of the observed decrease in $\delta^{15}N(NO_3^-)$ from 1850 to 1970 C.E.

1.6. Impacts of Postdepositional Processing. Ice core $\delta^{15}N(NO_3^-)$ is known to be affected by postdepositional processing. Postdepositional processing of snow nitrate is thought to be dominated by the photolysis of snow nitrate to NO_x (28), but is also influenced by evaporation of HNO_3 from the disorganized layer of snow grain surfaces (28, 29). In either case, nitrate remaining in snow is enriched in ^{15}N relative to the molecules [NO_x or $HNO_{3(g)}$] leaving snow. Therefore, changes in the degree of postdepositional processing will cause variations in ice core $\delta^{15}N(NO_3^-)$. The degree of postdepositional processing is influenced by snow accumulation rate which determines the residence time of nitrate in the photolytic zone (19), the abundance of light-absorbing impurities [i.e., black carbon (BC)] in snow which determines the penetration depth of UV actinic flux (30), and also snow acidity that promotes snow nitrate evaporation (28) and photolysis (31). Thus, either a snow accumulation rate increase, black carbon concentration increase, or snow acidity decrease from 1850 to 1970 could cause decrease in $\delta^{15}N(NO_3^-)$ during the same time period by limiting postdepositional loss. The snow accumulation rate at Summit stays relatively constant in the last ~200 y (Fig. S2*A*), ice core BC concentrations increased from ~1850 to 1920 and decreased afterward (14), and snow acidity increased from 1850 to 1970 (Fig. 2*A*). Although the large $\delta^{15}N(NO_3^-)$ values observed in Greenland snow deposited before 1850 relative to natural NO_x sources (Table S1) suggest that postdepositional processing is influencing the Greenland ice core nitrate record, variations in postdepositional processing due to changes in snow accumulation, UV absorbing impurities in the snow, or snow acidity cannot explain the observed long-term decrease in $\delta^{15}N(NO_3^-)$ from 1850 to 1970. The increase in BC concentrations from 1850 to ~1920 may contribute to the decrease in $\delta^{15}N(NO_3^-)$ during this period. However, the effect of BC on the degree of postdepositional processing of snow nitrate is small. Snow impurities, including BC, influence the postdepositional processing of snow nitrate through absorbing UV radiation, reducing the radiation in the snow for the photolysis of snow nitrate that occurs between wavelengths of 300 and 320 nm (32). However, the absorption of UV radiation in snow is dominated (>85%) by non-BC material such as HULIS and dust (30, 33), with BC accounting for the rest of the absorption of UV radiation (<15%). Although BC concentration increased from ~1850 to ~1920 due to industrial activities (coal combustion) (14), the increase in HULIS [represented by vanillic acid concentration, because vanillic acid and HULIS both originate mainly from biomass burning (34)] was not apparent (14). In addition, the concentration of dust [represented by Ca^{2+} concentration (Fig. S2*B*)] decreased from ~1850–1920. Therefore, it is unlikely that changes in postdepositional processing can account for the observed decrease in $\delta^{15}N$ from ~1850–1920.

1.7. Acidity Effect of Volcanic Eruptions. In case of atmospheric acidity arising from volcanic eruptions, one may expect similar decreases in $\delta^{15}N$ of ice core nitrate. We argue that the response of $\delta^{15}N$ of ice core nitrate depends primarily on the atmospheric acidity in the NO_x source regions. Unlike anthropogenic SO_2 sources, a volcanic eruption provides a single point source of SO_2 that is unlikely able to perturb the atmospheric acidity over the vast areas of NO_x sources (e.g., the North American continent). The reason that these eruptions have left apparent signals in the Greenland ice sheet (Fig. 2*B*) is because they are either local, tropospheric eruptions occurring in Arctic (i.e., 1912 Katmai, Alaska; 1946 Hekla, Iceland; 1783 Laki, Iceland) or explosive eruptions occurring in the tropics with a large effect on the stratosphere (i.e., 1991 Pinatubo, Indonesia; 1883 Krakatoa, Indonesia; 1835 Cosiguina, Nicaragua; 1831 Babuyan, Philippines; 1815 Tambora, Indonesia). Stratospheric-scale volcanic eruptions raise polar atmospheric acidity (as observed in this ice core) through stratospheric transport (i.e., Brewer–Dobson circulation) and the downwelling of air in the polar vortex (35), but they are unlikely to perturb the atmospheric acidity in midlatitudes, as evident by northern midlatitude ice core records that display no signal for neither the 1815 Tambora eruption nor the 1991 Pinatubo eruption

(36). Therefore, decreases in $\delta^{15}N$ of Greenland ice core nitrate are not expected in response to these eruptions via the mechanism proposed in this study. Indeed, for the periods corresponding to all of the major volcanic eruptions recorded in this ice core (Fig. 2*B*), including local, tropospheric eruptions and stratospheric-scale eruptions mentioned above except the 1815 Tambora and 1783 Laki eruptions, no decreases in $\delta^{15}N$ are seen (the ice covering the 1815 Tambora and 1783 Laki eruptions was used up before this study; thus we don't have $\delta^{15}N$ data for the period of these two events).

In sum, the relevant volcanic eruptions mentioned above raise Arctic atmospheric acidity, and thus Arctic snow acidity. Consequently, snow-sourced NO_x with low $\delta^{15}N$ in the Arctic should be enhanced during these episodic periods if acidity does indeed provide a significant control on the degree of snow nitrate photolysis. Meanwhile, the degree of postdepositional processing of snow nitrate at Summit is also enhanced due to snow acidity increase. The net isotopic effect of this process on ice core $\delta^{15}N$, as discussed earlier, depends on the net loss or gain of snow nitrate resulting in enrichment and depletion in $\delta^{15}N$, respectively. The fact that $\delta^{15}N$ of ice core nitrate shows no change in response to the above mentioned volcanic eruptions suggests that the effect of snow acidity changes on $\delta^{15}N$ due to possible enhancements of postdepositional processing of snow nitrate is negligible.

1. Jaegle L, Steinberger L, Martin RV, Chance K (2005) Global partitioning of NO_x sources using satellite observations: Relative roles of fossil fuel combustion, biomass burning and soil emissions. *Faraday Discuss* 130:407–423.
2. Rafter PA, Sigman DM, Charles CD, Kaiser J, Haug GH (2012) Subsurface tropical Pacific nitrogen isotopic composition of nitrate: Biogeochemical signals and their transport. *Global Biogeochem Cycles* 26:GB1003.
3. Salzmann R, Nussbaumer T (2001) Fuel staging for NO_x reduction in biomass combustion: Experiments and modeling. *Energy Fuels* 15(3):575–582.
4. Kendall C, Elliott EM, Wankel SD (2007) Tracing anthropogenic inputs of nitrogen to ecosystems. *Stable Isotopes in Ecology and Environmental Science*, eds Lajtha K, Michener RH (Blackwell Scientific Publications, Oxford), pp 375–449.
5. Spoelstra J, Schiff SL, Hazlett PW, Jeffries DS, Semkin RG (2007) The isotopic composition of nitrate produced from nitrification in a hardwood forest floor. *Geochim Cosmochim Acta* 71(15):3757–3771.
6. Morin S, et al. (2009) Comprehensive isotopic composition of atmospheric nitrate in the Atlantic Ocean boundary layer from 65°S to 79°N. *J Geophys Res* 114: D05303.
7. Elliott EM, et al. (2007) Nitrogen isotopes as indicators of NO_x source contributions to atmospheric nitrate deposition across the Midwestern and northeastern United States. *Environ Sci Technol* 41(22):7661–7667.
8. Ammann M, et al. (1999) Estimating the uptake of traffic-derived NO_2 from ^{15}N abundance in Norway spruce needles. *Oecologia* 118(2):124–131.
9. Moore H (1977) The isotopic composition of ammonia, nitrogen dioxide, and nitrate in the atmosphere. *Atmos Environ* 11(12):1239–1243.
10. Hastings MG, Jarvis JC, Steig EJ (2009) Anthropogenic impacts on nitrogen isotopes of ice-core nitrate. *Science* 324(5932):1288.
11. Felix JD, Elliott EM (2013) The agricultural history of human-nitrogen interactions as recorded in ice core $\delta^{15}N\text{-}NO_3^-$. *Geophys Res Lett* 40(8):1642–1646.
12. Holtgrieve GW, et al. (2011) A coherent signature of anthropogenic nitrogen deposition to remote watersheds of the Northern Hemisphere. *Science* 334(6062): 1545–1548.
13. Pasteris DR, McConnell JR, Edwards R (2012) High-resolution, continuous method for measurement of acidity in ice cores. *Environ Sci Technol* 46(3):1659–1666.
14. McConnell JR, et al. (2007) 20th-century industrial black carbon emissions altered Arctic climate forcing. *Science* 317(5843):1381–1384.
15. Legrand M, Mayewski P (1997) Glaciochemistry of polar ice cores: A review. *Rev Geophys* 35(3):219–243.
16. Seinfeld JH, Pandis SN (2006) *Atmospheric Chemistry and Physics: From Air Pollution to Climate Change* (Wiley, New York), 2nd Ed.
17. Keene WC, Pszenny AAP, Maben JR, Stevenson E, Wall A (2004) Closure evaluation of size-resolved aerosol pH in the New England coastal atmosphere during summer. *J Geophys Res* 109:D23307.
18. Kajino M (2003) *Modelling Liquid Water Content of Atmospheric Aerosols* (Internation Institute for Applied Systems Analysis, Laxenburg, Austria).
19. Erbland J, et al. (2013) Air–snow transfer of nitrate on the East Antarctic Plateau - Part 1: Isotopic evidence for a photolytically driven dynamic equilibrium. *Atmos Chem Phys* 13:6403–6419.
20. Heaton THE, Spiro B, Madeline S, Robertson C (1997) Potential canopy influences on the isotopic composition of nitrogen and sulphur in atmospheric deposition. *Oecologia* 109(4):600–607.
21. Fountoukis C, Nenes A (2007) ISORROPIA II: A computationally efficient thermodynamic equilibrium model for $K^+\text{-}Ca^{2+}\text{-}Mg^{2+}\text{-}NH_4^+\text{-}Na^+\text{-}SO_4^{2-}\text{-}NO_3^-\text{-}Cl^-\text{-}H_2O$ aerosols. *Atmos Chem Phys* 7(17):4639–4659.
22. Wolff EW (2013) Ice sheets and nitrogen. *Philos Trans R Soc B* 368(1621):20130127.
23. Lamarque JF, et al. (2010) Historical (1850–2000) gridded anthropogenic and biomass burning emissions of reactive gases and aerosols: Methodology and application. *Atmos Chem Phys* 10(15):7017–7039.
24. Jarvis JC, Steig EJ, Hastings MG, Kunasek SA (2008) Influence of local photochemistry on isotopes of nitrate in Greenland snow. *Geophys Res Lett* 35(21):L21804.
25. Freyer HD, Kley D, Volzthomas A, Kobel K (1993) On the interaction of isotopic exchange processes with photochemical reactions in atmospheric oxides of nitrogen. *J Geophys Res* 98(D8):14791–14796.
26. Alexander B, et al. (2009) Quantifying atmospheric nitrate formation pathways based on a global model of the oxygen isotopic composition ($\Delta^{17}O$) of atmospheric nitrate. *Atmos Chem Phys* 9(14):5043–5056.
27. Sofen ED, Alexander B, Kunasek SA (2011) The impact of anthropogenic emissions on atmospheric sulfate production pathways, oxidants, and ice core $\Delta^{17}O\ SO_4^{2-}$. *Atmos Chem Phys* 11(7):3565–3578.
28. Frey MM, Savarino J, Morin S, Erbland J, Martins JMF (2009) Photolysis imprint in the nitrate stable isotope signal in snow and atmosphere of East Antarctica and implications for reactive nitrogen cycling. *Atmos Chem Phys* 9(22):8681–8696.
29. Blunier T, Floch GL, Jacobi HW, Quansah E (2005) Isotopic view on nitrate loss in Antarctic surface snow. *Geophys Res Lett* 32(13):L13501.
30. Zatko MC, et al. (2013) The influence of snow grain size and impurities on the vertical profiles of actinic flux and associated NO_x emissions on the Antarctic and Greenland ice sheets. *Atmos Chem Phys* 13(7):3547–3567.
31. Abida O, Osthoff HD (2011) On the pH dependence of photo-induced volatilization of nitrogen oxides from frozen solutions containing nitrate. *Geophys Res Lett* 38:L16808.
32. Chu L, Anastasio C (2003) Quantum yields of hydroxyl radical and nitrogen dioxide from the photolysis of nitrate on ice. *J Phys Chem A* 107(45):9594–9602.
33. Beine H, et al. (2011) Soluble, light-absorbing species in snow at Barrow, Alaska. *J Geophys Res* 116:D00R05.
34. Lin P, Engling G, Yu JZ (2010) Humic-like substances in fresh emissions of rice straw burning and in ambient aerosols in the Pearl River Delta Region, China. *Atmos Chem Phys* 10(14):6487–6500.
35. Holton JR, et al. (1995) Stratosphere-troposphere exchange. *Rev Geophys* 33(4):403–439.
36. Kaspari S, et al. (2009) Recent increases in atmospheric concentrations of Bi, U, Cs, S and Ca from a 350-year Mount Everest ice core record. *J Geophys Res* 114:D04302.

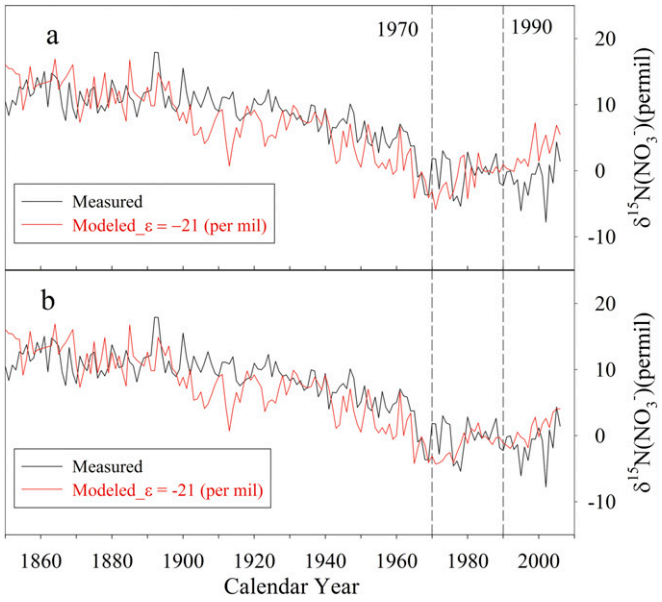

Fig. S1. Effect of the potential difference in the trends in SO_2 emissions and ice core sulfate concentrations after ~1990 on the model result. (*A*) The acidity used in the model is calculated from measured ice core ion concentrations throughout the record (*B*) When calculating the acidity, sulfate concentrations after 1970 are scaled according to SO_2 emission data (see main text for more details).

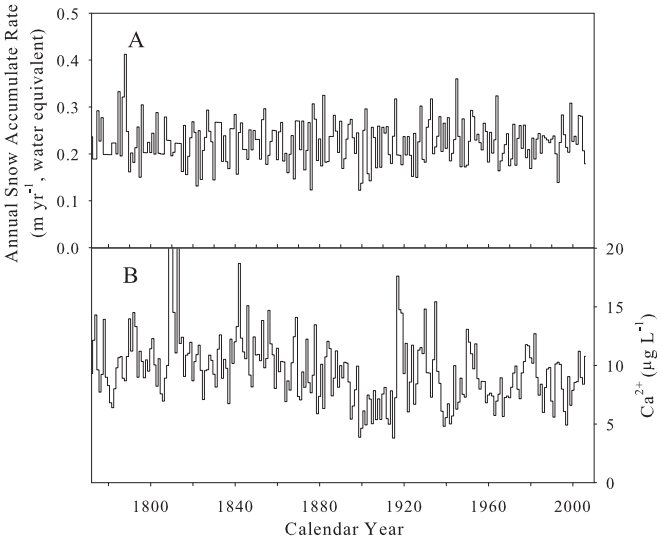

Fig. S2. (*A*) Annual snow accumulation rate (in water equivalent size) and (*B*) snow calcium concentration from 1772 to 2006 at Summit, Greenland.

Table S1. Values of $\delta^{15}N$ of NO_x from various sources

Sources		$\delta^{15}N$, ‰, vs. N_2	References
Coal combustion	Coal power plant	6–13	(1)
		9.2–25.6	(2)
	Heating source	*–5.3*	(3)
Petroleum combustion	Vehicle emission	*–13 to –2*	(1)
		5.7 ± 2.8	(4)
		3.9–5.4	(3)
		3.4–3.9	(5)
	Heating source	*–19.4* to 2.9	(3)
Natural gas combustion	Heating source	3.0–15.4	(3)
Waste incinerators		5.5–8.0	(3)
Soil emissions	*N*-fertilized soil	–48.9 to –19.9	(6)
	Unfertilized soil	–9.3 ± 3.5	(5)
Lightning		–0.5–1.4	(7)
Biomass burning		<0*	
Snow nitrate photolysis		–50 to –20†	

Darker shading represents anthropogenic sources, while lighter shading distinguishes the biogenic process affected by synthesized *N*-fertilizer.

*Predicted to be negative, see *SI Text*.

†Predicted from $\delta^{15}N$ measurement of atmospheric boundary layer nitrate in snow-covered areas (28).

1. Heaton THE (1990) 15N/14N ratios of NOx from vehicle engines and coal-fired power stations. *Tellus B* 42(3):304–307.
2. Felix JD, Elliott EM, Shaw SL (2012) Nitrogen Isotopic Composition of Coal-Fired Power Plant NOx: Influence of Emission Controls and Implications for Global Emission Inventories. *Environ Sci Technol* 46(6):3528–3535.
3. Widory D (2007) Nitrogen isotopes: Tracers of origin and processes affecting PM10 in the atmosphere of Paris. *Atmos Environ* 41(11):2382–2390.
4. Ammann M, et al. (1999) Estimating the uptake of traffic-derived NO2 from 15N abundance in Norway spruce needles. *Oecologia* 118(2):124–131.
5. Moore H (1977) The isotopic composition of ammonia, nitrogen dioxide, and nitrate in the atmosphere. *Atmos Environ* 11(12):1239–1243.
6. Li DJ, Wang XM (2008) Nitrogen isotopic signature of soil-released nitric oxide (NO) after fertilizer application. *Atmos Environ* 42(19):4747–4754.
7. Hoering T (1957) The isotopic composition of the ammonia and the nitrate ion in rain. *Geochim Cosmochim Ac* 12:97–102.

Other Supporting Information Files

Dataset S1 (PDF)